Springer

Acta Mechanica Sinica

CrossMark click for updates

• RESEARCH PAPER •

Acta Mech. Sin., Vol. 41, 324496 (2025)
https://doi.org/10.1007/s10409-024-24496-x

Effect of morphological profile of dandelion-seed on flight lift force under crosswind

Lang Qin[1], Huasong Qin[1*], and Lifeng Ma[1,2*]

[1] *State Key Laboratory for Strength and Vibration of Mechanical Structures, Department of Engineering Mechanics, Xi'an Jiaotong University, Xi'an 710049, China;*

[2] *Department of Mechanical, Materials and Manufacturing Engineering, University of Nottingham, Nottingham NG7 2RD, UK*

Received August 26, 2024; accepted September 24, 2024; published online April 30, 2025

In this paper, the effect of the morphological profile of dandelion seed on flight lift force under crosswind conditions is explored. Existing studies primarily focus on the flight characteristics of dandelion seed during its fall, emphasizing the influence of the complex filament structure on the formation of wake vortices. However, research on the flight lift force due to the dandelion seed's morphological profile under lateral crosswind conditions is quite limited. This study investigates the aerodynamic behavior of dandelion seed using a novel virtual barrier model. This model is proposed, based on the regular pattern of the filaments' outer contours and the virtual barrier effect produced by their columnar array. Through elaborate numerical simulations, it is found that the morphological profile of dandelion seed possesses superior aerodynamic properties, particularly in generating lift force under crosswind conditions. This characteristic is a crucial mechanism for the long-distance dispersal of dandelion seed. Subsequently, the study extends to examine the aerodynamic performance of the model at varying degrees of opening angles and inflow attack angles, offering a fresh perspective on understanding the flight characteristics of dandelion seed in natural environments. The findings not only contribute to the field of plant aerodynamics but also provide insights into potential biomimetic applications in engineering.

Dandelion seed, Virtual fluid barrier, Flight ability, Vortex

Citation: L. Qin, H. Qin, and L. Ma, Effect of morphological profile of dandelion-seed on flight lift force under crosswind, Acta Mech. Sin. 41, 324496 (2025), https://doi.org/10.1007/s10409-024-24496-x

1. Introduction

It is a highly effective approach in research and application to draw inspiration from nature. The unique falling mechanism of maple samaras [1] and the flapping flight [2,3] of insects like dragonflies [4] provide valuable research material, offering significant insights for academic studies and practical innovations. Seed dispersal mechanisms play a vital role in the continuation and propagation of species in the natural world [5,6]. These mechanisms [7] exhibit the variety and complexity inherent in natural selection. Seeds employ multiple strategies for dispersal to new growth areas, including the use of external forces like wind, water currents, and animals, along with their specific structures and functionalities. Among many dispersal strategies, wind dispersal has attracted great interest from scientists because of its unique biomechanical properties and its suitability for long-range dispersal [8-10]. Especially the dandelion seeds, which possess an efficient ability to disperse through the air and a unique flying mechanism, have made them a center of interest in the studies of biomechanics and biomimicry.

The architecture of dandelion seed is notably intriguing. The pappus of a dandelion seed consists of about a hundred slender filaments, radially arranged from the center outward, forming a structure with high porosity. This unique structure significantly reduces the seed's specific density. This distinctive structural characteristic is critical in their flight dispersion. The wind tunnel experiments conducted by Cummins et al. [11] showed that vertical airflows lead to the

*Corresponding authors. E-mail addresses: huasongqin@xjtu.edu.cn (Huasong Qin); malf@mail.xjtu.edu.cn (Lifeng Ma)
Executive Editor: Yue Yang

formation of vortices above dandelion seed, underscoring the significance of this structure for flight stability. Furthermore, Qiu et al. [12] investigated the impact of porosity on vortex ring stability, revealing that stable vortex rings form at the seed's tail only when the porosity does not exceed a certain threshold. By utilizing particle image velocimetry (PIV), Shigenaga and Hasegawa [13] studied the flow field characteristics during the descent of dandelion seed. Their research indicates that the descent speed of dandelion seed is significantly influenced by their orientation, which remarkedly affects the seed's aerodynamic properties. Also, Meng et al. [14] and Seale et al. [15] studied how air humidity influences the opening angles of dandelion pappi and its effects on the seed's aerodynamic drag. Under low humidity conditions, the expansion angle of dandelion pappi enlarges, resulting in a fluffier seed and enhanced aerodynamic drag. In addition, taking into account the deformation of dandelion filaments, Sun and Guo [16] simulated the aerodynamic behaviors of the filaments in fluids.

On the other hand, several researchers have studied the flying stability of dandelion seed. Qin et al. [17] studied the flight stability of dandelions when their axis is not aligned with the vertical direction, analyzing the effect of different opening angles on posture stability through numerical simulation. The research shows that, when the folding angle ranges from 20° to 40°, the dandelion achieves optimal posture stability and drag coefficient. By utilizing linear stability analysis, Ledda et al. [18] studied the aerodynamic characteristics of dandelions under vertical flow conditions, focusing particularly on the stability of wake structures and the impact of the pappus structure on drag. Dong et al. [19] conducted transient simulation studies on the transition of dandelion wakes from stable to unstable and then to turbulent at different Reynolds numbers. This study reveals that, in comparison with solid disks, the high porosity of dandelion pappi is able to raise the threshold value to achieve a stable flight.

So far, most studies in literature mainly focused on the flight mechanism of dandelion seed and have been limited to the case of dandelion seed in free fall. Research on the flight aerodynamic characteristics of dandelion seed, due to its morphological profile, under complex wind conditions is quite limited. Especially, the flight aerodynamic behavior of a dandelion seed under a lateral horizontal crosswind condition has not been reported, whilst this scenario is believed to mainly account for its long-distance autonomic flight. Addressing these issues is crucial for a deeper understanding of dandelion seed flight mechanics and advancing the development of biomimetic applications.

The aim of this study is to explore the effect of morphological profile of dandelion seed on the flight lift force under complicated wind conditions, particularly lateral crosswind conditions. Using a virtual barrier model based on the dandelion seed profile, this work primarily investigates: (I) how variations in the geometric parameters of the model affect the dandelion's aerodynamic performance and flow field under horizontal inflow; (II) how inflow angle influences the aerodynamic performance and flow field of the dandelion with typical geometric parameters of the model. It is expected that this study will reveal intriguing mechanisms for the design of dandelion-like flying devices.

2. Numerical setup

2.1 Dandelion's "virtual barrier" model and computational domain

As shown in Fig. 1(a), the pappus structure of natural dandelion seed is a highly complex three-dimensional structure.

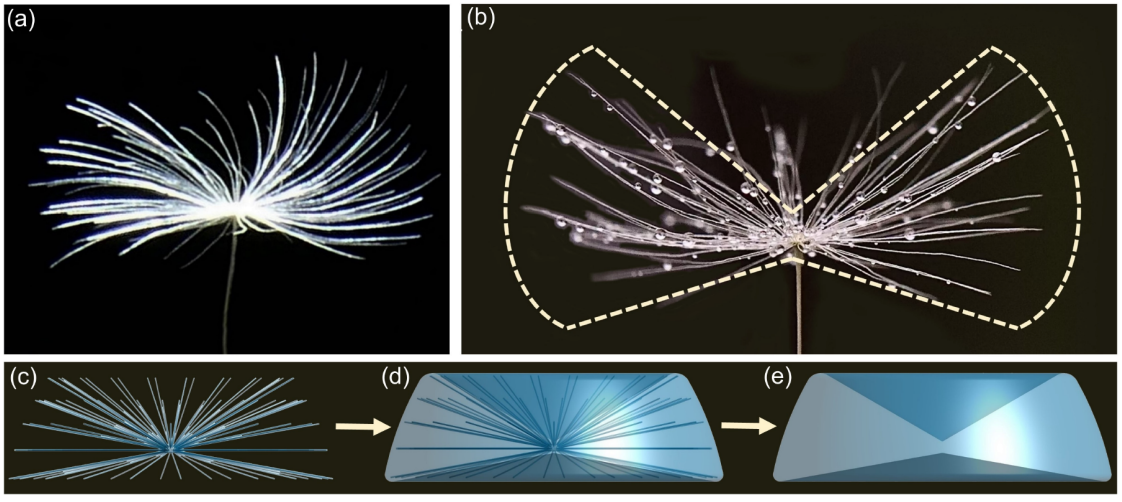

Figure 1 (a) Photo of dandelion seed; (b) the contour line of the dandelion's outer edge; (c) dandelion multi-filament model; (d) outer structure of the dandelion filament model; (e) dandelion virtual barrier model.

On the one side, previous studies have indicated that the presence of elongated columnar arrays impedes the passage of air. On the other side, it is believed that a major feature of the dandelion's filament structure is its significantly reduced specific density, resulting in an easy float in the air. Also, the outer morphological profile of dandelion seed resembles a donut-like structure shown in Fig. 1(b), which is supposed to be closely related to the aerodynamic performance of dandelion seed. In order to investigate the aerodynamic behavior of a dandelion seed with such a structural morphology shown in Fig. 1, firstly, we develop a model that may sufficiently represent the filament structure of the dandelion seed, as depicted in Fig. 1. A practical structure may be shown in Fig. 1(c). The periphery of the dandelion's filament structure is enclosed with a thin wall, tightly fitting to the outer edges of the petioles at the upper and lower parts of the dandelion as shown in Fig. 1(d). The space enclosed by the thin wall forms a solid axisymmetric donut-like structure, which is referred to as the virtual barrier model in this study (Fig. 1(e)). This virtual barrier model may directly represent the main pappus edge structure characteristics of the dandelion seed. It will be used to study the effect of morphological profile of a dandelion seed on its aerodynamic behavior, especially, on the flight lift force, when it is subjected to crosswinds.

Before proceeding, a justification for the virtual barrier model of the dandelion seed pappus is presented as follows. In Refs. [20-23], similar to the filamentous structures of dandelion seed, the comb-like wing structures of certain insects have attracted widespread research interest. The flight mechanics and aerodynamic capabilities of these insects have been investigated [24-27]. Lee and Kim [28] and Lee et al. [29] simplified bristle wings into a two-dimensional circular array and numerically studied the aerodynamic characteristics of bristle wings under intermittent wind loads. They found that the airflow transmission rate between the bristle arrays was extremely low, and then they proposed the concept of a "virtual barrier", which, later, was proved to be efficient and powerful in numerical simulations. Lee et al. [30] found that the virtual barrier effect of the pyroclastic cluster structure in dandelions obstructs the permeable fluid flow between these structures. Because the structure of the dandelion pappus is quite similar to that of a comb-like wing, thus, the concept of the "virtual barrier" related to columnar arrays is literally adapted to the study of the aerodynamic characteristics of dandelion seed. Based on the structural characteristics of the dandelion seed pappus, the outer edge wall of the dandelion pappus is treated as a whole as shown in Fig. 1(e), providing a simple way to simulate the flight aerodynamic behavior of dandelion seed.

Figure 2(a) depicts the cross-section of the virtual barrier model. The radius of the uppermost filament is R_1 and the radius of the lowermost filament is R_2. The angle α is formed between the uppermost filament and the horizontal plane, and the angle β is formed between the lowermost filament and the horizontal plane, and the total angle of the virtual barrier model is $\theta = \alpha + \beta$. The radius $R_3 = (R_1 + R_2)/2$ represents the radius of the interpolating arc a_1 between R_1 and R_2, and the arcs are tangentially connected. Based on these key parameters the contour of the outer edge of the dandelion filament can be determined. After rotating around the Z-axis, the virtual barrier dandelion model shown in Fig. 2(b) is obtained. By using this method, the aerodynamic characteristics of the virtual obstacle dandelion model can be studied with the change of α and β angles.

In this study, the maximum diameter projection length of the dandelion virtual barrier model, designated as D, is established at 10 mm in the model. The computational domain is shown in Fig. 3. To ensure sufficient fluid flow within the computational domain, the distances from the dandelion to the domain's inlet and outlet are set at $8D$ and $12D$, respectively. The boundary of the computational domain is defined as a cylindrical surface at $8D$ from the dandelion. The domain's inlet is set as a velocity inlet, and the outlet is set as a pressure outlet.

The uniform velocity boundary condition is imposed at the inlet, and the pressure outlet boundary condition is imposed at the outlet. The inlet uniform velocity is larger than zero. Both the surface of the dandelion and the cylindrical boundary are set as non-slip surfaces. Air is set as an incompressible ideal gas, the air density $\rho = 1.204\ \mathrm{kg/m^3}$, the viscosity constant of $\mu = 1.511 \times 10^{-7}\ \mathrm{Pa{\cdot}s}$. Reynolds number is defined as

$$Re = \frac{\rho U D}{\mu}, \tag{1}$$

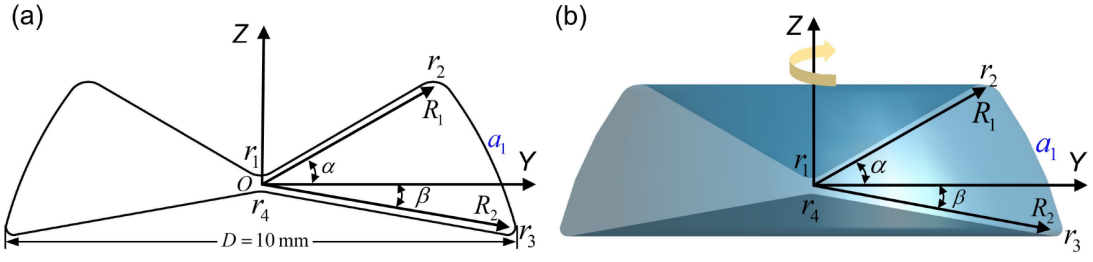

Figure 2 (a) 2D planar diagram of the dandelion virtual barrier model, (b) 3D view of the dandelion virtual barrier model.

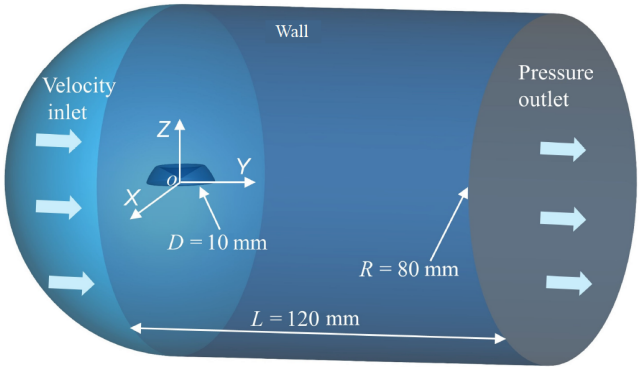

Figure 3 Fluid domain and boundary conditions in this study.

where D is the model projected diameter, and U is the inflow velocity of the airflow.

2.2 Flow control equations and turbulence model

The continuity equation for incompressible flow can be expressed as

$$\nabla \cdot \mathbf{u} = 0, \tag{2}$$

where $\mathbf{u}$ is the velocity vector. Additionally, the Navier-Stokes equations are used to model the motion of the fluid. For incompressible flow in the absence of external forces, the Navier-Stokes equations reduce to

$$\rho(\partial \mathbf{u}/\partial t + \mathbf{u} \cdot \nabla \mathbf{u}) = -\nabla p + \mu \nabla^2 \mathbf{u}, \tag{3}$$

where ρ is the fluid density, t is time, p is the pressure, μ is the fluid's dynamic viscosity, and $\nabla^2 \mathbf{u}$ is the Laplacian of the velocity field. With appropriate boundary conditions, this equation can be solved to obtain the velocity field of the fluid surrounding the dandelion.

The Laminar model is employed to simulate the steady-state flow. The numerical algorithm utilizes the Coupled methodology, incorporating the Rhie-Chow interpolation scheme to prevent the decoupling of velocity and pressure fields. The process of establishing discrete equations necessitates the careful selection of an appropriate discretization scheme for each term presented within the equations. In this study, the second-order upwind scheme is employed to discretize the terms of the control equation. A convergence criterion has been established, stipulating that computational residuals must be less than 10^{-4} to ensure the accuracy and reliability of the results.

3. Results and discussion

We focus our discussion on two aspects: (I) the influence of the dandelion's upper and lower edge angles, α and β, on its vortex structure and air drag; (II) the stability of the dandelion's posture under the deflection angle between its axial direction and the flow direction.

3.1 Effect of the characteristic angles of the dandelion virtual barrier model on the flow field

To verify the effectiveness of the dandelion virtual barrier model, computational fluid dynamics (CFD) technology is employed here to obtain the flow field of the dandelion virtual barrier model under vertical inflow. It can be seen that under vertical inflow, the PIV flow field of the real dandelion (Fig. 4(a)) is very similar to the flow field obtained from the simulation calculation (Fig. 4(b)). This may confirm the validity of the virtual barrier model. The primary reason for the vortex structure of the virtual barrier model not separating from the model is that the porosity of

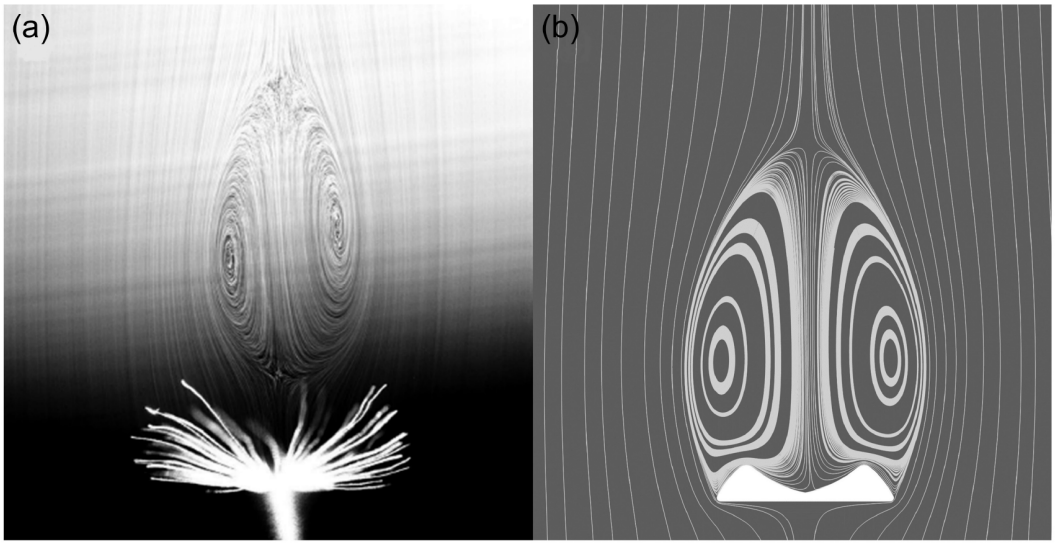

Figure 4 (a) PIV images of dandelion flow field [11]; (b) the simulated virtual barrier model flow field.

the virtual barrier model differs to some extent from that of the real dandelion. For the comprehensive study of the aerodynamic performance of dandelions, the virtual barrier model can significantly reduce computational costs.

As illustrated in Fig. 5, the flow field analysis of the virtual barrier model under horizontal inflow conditions highlights its distinctive aerodynamic features. A primary vortex is generated in the recessed area of the model, and a secondary vortex appears in the downstream wake. The primary vortex forms as a result of fluid deceleration and the corresponding pressure rise within the recessed region, while the secondary vortex is linked to the fluid recirculation in the wake of the primary vortex. The existence of these vortex structures is crucial for simulating the flight stability of dandelion seeds in horizontal airflow and deserves further detailed study.

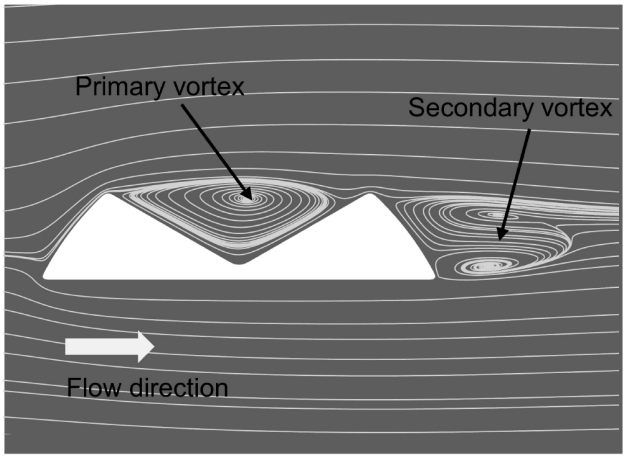

Figure 5 Flow field of the virtual barrier model under horizontal crosswind.

Figure 6 shows the pressure contour distribution of the dandelion virtual barrier model at $Re = 250$ with a horizontal wind direction at a fixed angle of $\beta = -5°$ in different α angles. The darker regions represent high-pressure areas, while the lighter regions represent low-pressure areas. As α angle increases, the area of the high-pressure zone gradually expands, while the shape and size of the low-pressure zone also change. Regardless of the changes in the α angle, low-pressure zones consistently exist in the groove area and at the model's tail, although their specific distribution adjusts with changes in the α angle. These changes in pressure distribution have a significant impact on the aerodynamic characteristics and lift generation ability of the model, further supporting the possibility of long-distance dispersal of dandelion seeds.

To further understand the impact of varying α angles on the pressure distribution across a specific plane on the model's surface, Fig. 7 presents the distribution of surface pressure coefficients at the $X = 0$ plane for different α angles, with β set to $-5°$. The pressure coefficient C_P is defined as $C_p = \frac{(p - p_\infty)}{0.5\rho U^2}$, where p represents the pressure at the monitoring point, and p_∞ is the freestream static pressure. The pressure coefficient curves indicate a complex pressure distribution on the surface at this plane, with

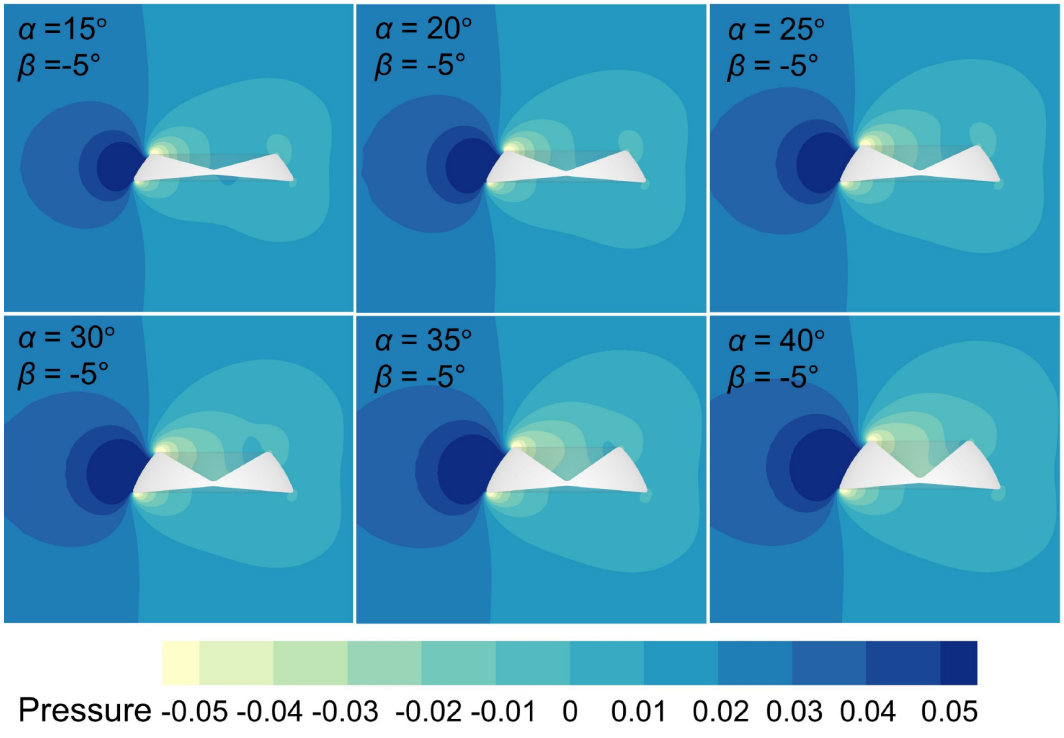

Figure 6 Pressure distribution of the virtual barrier model at different α angles with Reynolds number $Re = 250$.

multiple negative pressure peaks. It is noteworthy that the upper surface of the model contains multiple negative pressure regions (where C_P is positive), which are the primary contributors to the model's lift. In contrast, the front end and lower surface of the model mainly exhibit positive pressure regions (where C_P is negative). The area integral of the pressure curve, using $C_P = 0$ as the reference, reaches its peak around $\alpha = 30°$, which corresponds to the maximum lift.

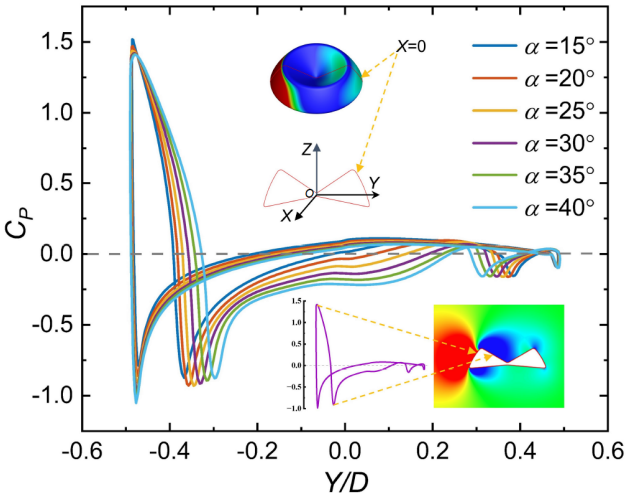

Figure 7 Pressure coefficient curves of the dandelion virtual barrier model at different α angles on the $X = 0$ plane.

Figure 8 depicts the drag coefficient C_D curves for the model under different speeds, α and β angles, where $C_D = \dfrac{F_D}{0.5\rho U^2 A}$, F_D is the drag force acting on the model, and A is the reference area of the model. It can be observed that as the horizontal flow speed increases (Re increases), the drag coefficient decreases gradually across different models (varying α angles). Notably, as the same Re, the drag coefficient is relatively higher when $\alpha = 15°$, and relatively lower when $\alpha = 40°$, indicating that under the same β angle and inflow speed, increasing the α angle will cause the drag coefficient of the model to decrease. When α angle is fixed, the drag coefficient also decreases progressively as β decreases.

In Fig. 9(a), when $\beta = 5°$, the lift coefficient of all models

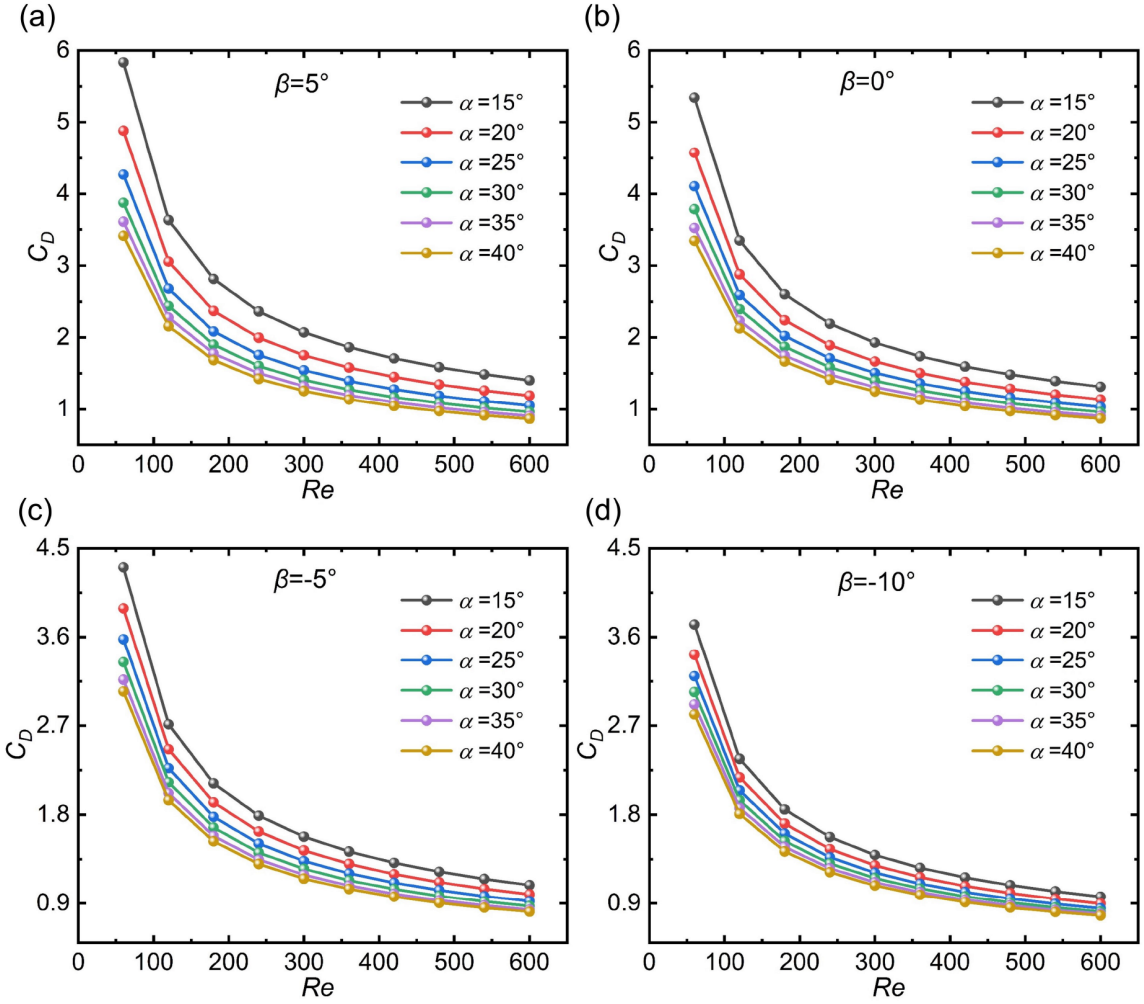

Figure 8 Drag coefficient variation with Re at different α and β angles, (a) $\beta = 5°$, (b) $\beta = 0°$, (c) $\beta = -5°$, and (d) $\beta = -10°$.

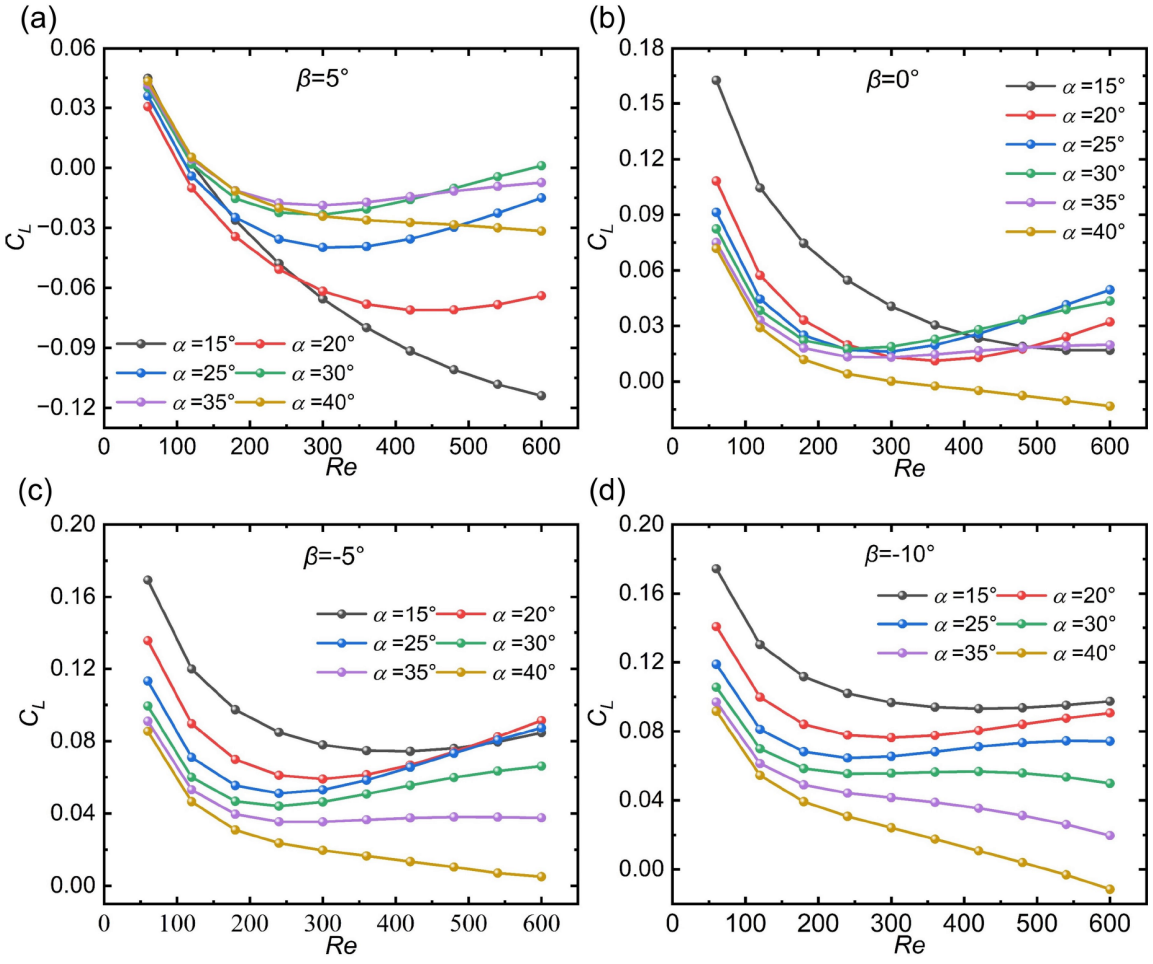

Figure 9 Lift coefficient variation with Reynolds numbers at different α and β angles. (a) β = 5°; (b) β = 0°; (c) β = −5°; (d) β = −10°.

is relatively small, with some models even having negative lift coefficients at higher Reynolds numbers. This indicates that at β = 5°, the models are unable to generate sufficient lift from the natural airflow, and some models even descend faster under stronger inflow. From Fig. 9(b), it can be seen that the lift coefficient of the seen that the lift coefficients for the models at β = 0° have significantly increased compared to those at β = 5°. As the Reynolds number increases, the lift coefficients of most models in this group either gradually decrease or stabilize (α = 15°, α = 35°, α = 40°). Some models exhibit a decrease in lift coefficient followed by an increase as *Re* continues to rise (α = 20°, α = 25°, α = 30°). Figure 9(c) shows that at β = −5°, the lift coefficients of the models have further increased compared to those at β = 0°. The trend in lift coefficient variation with Reynolds number for different α angles is similar to that at β = 0°. In Fig. 9(d), when β = −10°, the lift coefficients of the models further increase compared to β = −5° at the same Reynolds number. For most models, the lift coefficient first decreases and then either stabilizes or slightly increases as the Reynolds number rises, while in some cases, the lift coefficient continues to decrease.

In general, the variation in lift coefficients for models with different β and α angles across various Reynolds numbers is extremely complex. For aircraft design, the goal is to achieve good lift coefficient performance across different Reynolds numbers. This is to ensure that the model can adapt to the complex wind conditions in natural environments. Considering the drag coefficients of various models at different Reynolds numbers, it has been observed that at β = −10°-0°and α = 25°-30°, the models exhibit both low drag coefficients and high lift coefficients. This can be used as a reference to design biomimetic micro aerial vehicles with excellent aerodynamic performance.

3.2 The influence of the flow attack angle on the dandelion's aerodynamic properties

In natural environments, it is rare for the symmetry axis of a falling dandelion to align perfectly parallel to the vertical direction. This research further investigates the aerodynamic properties of the model as it descends in different orientations and, at the same time, is subjected to horizontal inflow. Here we define a key parameter φ, which is the angle of

attack between the inflow direction and the plane perpendicular to the symmetry axis of the dandelion model. The effects of variation φ on the model and the surrounding flow field, as well as its impact on the model's lift and drag forces, are explored. As shown in Fig. 10, it shows that when $\varphi > 0°$, the axis of symmetry of the dandelion is no longer parallel to the vertical direction. As a result, the dandelion's center of gravity no longer aligns with its symmetry axis, generating a torque that seeks to reorient the model to align with the axis of gravity. Moreover, it shows that two low-pressure zones develop on the upper side of the dandelion virtual barrier model and a high-pressure zone on the lower side. The pressure difference between the upper and lower sides offers the lift force to the model. The high-pressure area on the windward front also creates a torque that causes the dandelion's symmetry axis to deviate from the vertical, which may balance with the torque generated by its gravity G.

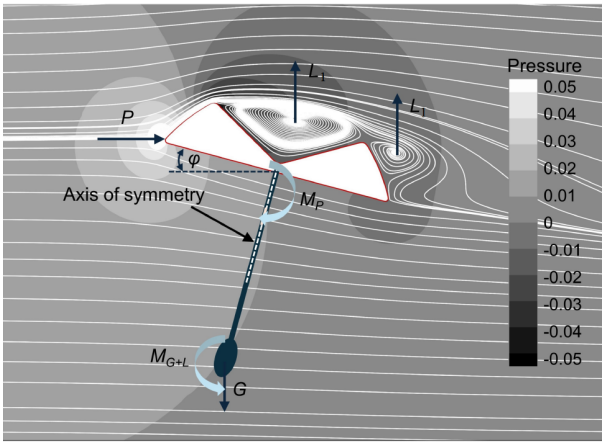

Figure 10 Analysis of mechanical forces in the flow field for the virtual barrier model at angle of attack $\varphi > 0°$.

Figure 11 illustrates the pressure distribution of the virtual barrier model at different angles of attack φ, under the conditions of $Re = 250$, $\alpha = 30°$, and $\beta = -5°$. As the angle of attack φ increases, the pressure distribution on the model's surface changes significantly. Specifically, a low-pressure zone gradually forms in the recessed area of the model's upper surface, indicating that as the angle of attack increases, airflow accelerates in this region, leading to a pressure drop consistent with Bernoulli's principle. Meanwhile, the high-pressure zones on the lower surface and leading edge of the model gradually expand, reflecting the deceleration of airflow in these regions and the corresponding increase in pressure. Particularly in the lower left area of the model, the airflow is more significantly obstructed, leading to a further increase in pressure. These changes in the distribution of high- and low-pressure zones directly affect the model's aerodynamic performance, particularly in terms of lift and drag characteristics. By adjusting the angle of attack, the aerodynamic performance of the model can be optimized. Figure 11 provides a clear basis for understanding how changes in the angle of attack affect pressure distribution and aerodynamic performance.

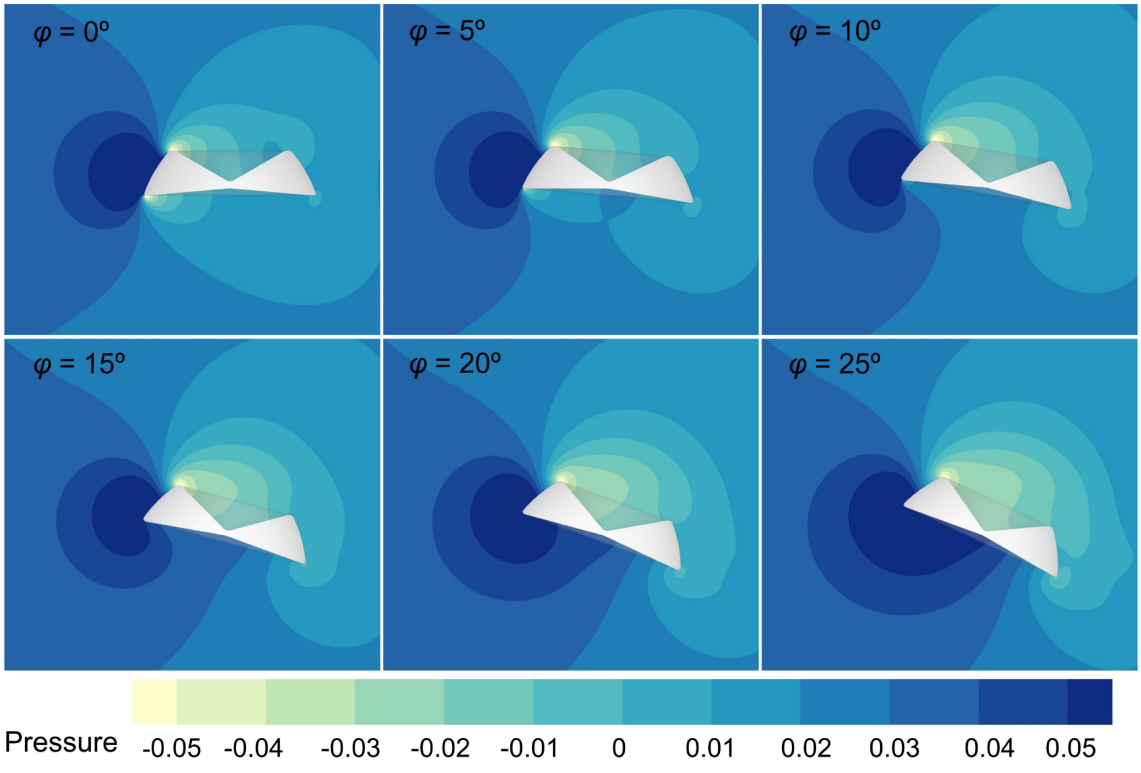

Figure 11 Pressure distribution of the virtual barrier model at different angles of attack φ with $Re = 250$, $\alpha = 30°$, and $\beta = -5°$.

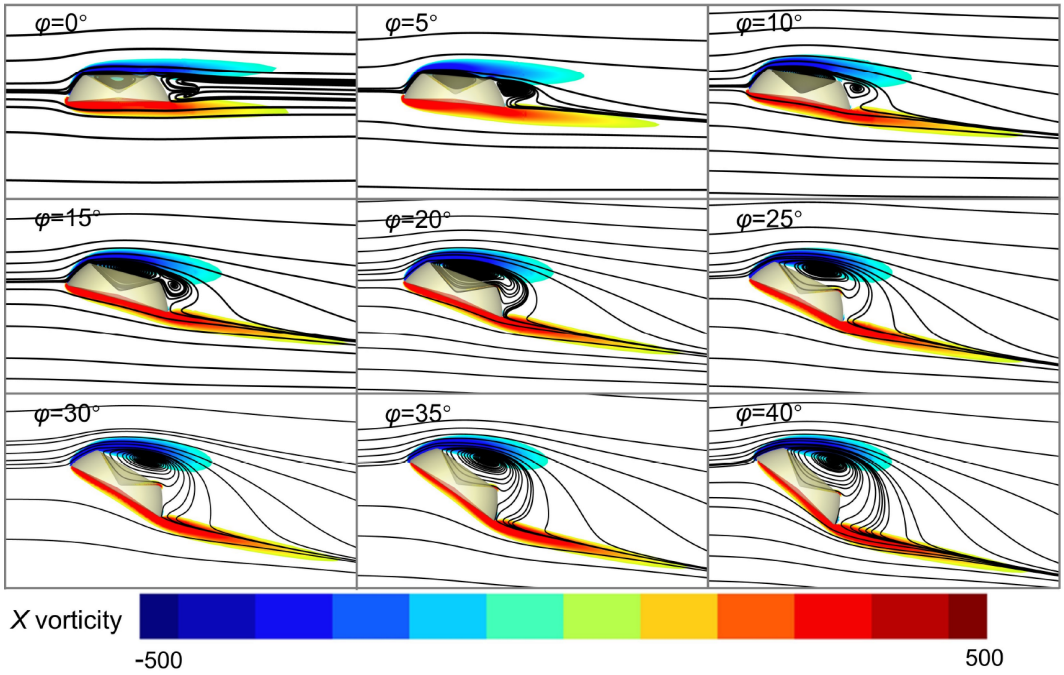

Figure 12 Vorticity contour in the *X*-direction and streamlines for different angles of attack.

Figure 12 shows the *X*-direction vorticity contour plots of the model at $\alpha = 30°$, $\beta = -5°$ under different angles of attack, specifically highlighting the positive and negative vorticity within the ranges of [−500, −50] and (50, 500], while excluding values in the range of [−50, 50]. As depicted in Fig. 12, with an increase in the angle of attack, the primary vortex intensifies, whereas the secondary vortex diminishes and eventually vanishes. This phenomenon occurs because the concave characteristics of the model enhance airflow adhesion to the upper surface, reducing the probability of flow separation. Consequently, this design provides the model with a larger stall angle compared to conventional wing structures. The vortex structures present on the model's surface effectively form a new equivalent wing structure. These vortices prevent direct interaction between the free airflow and the model surface, causing relative displacement between the free airflow and the vortex structures. This situation converts air-solid friction into air-air friction, akin to a "rolling bearing" mechanism, thus contributing to the reduction of viscous drag.

Figure 13 illustrates the model's drag force, lift force, and lift-to-drag ratio (C_L/C_D) as a function of the attack angle. Figure 13(a) shows that the lift coefficient increases initially with the attack angle, reaches a peak around 35°, and then gradually decreases. The attack angle at which the peak occurs corresponds to the stall angle of the model,

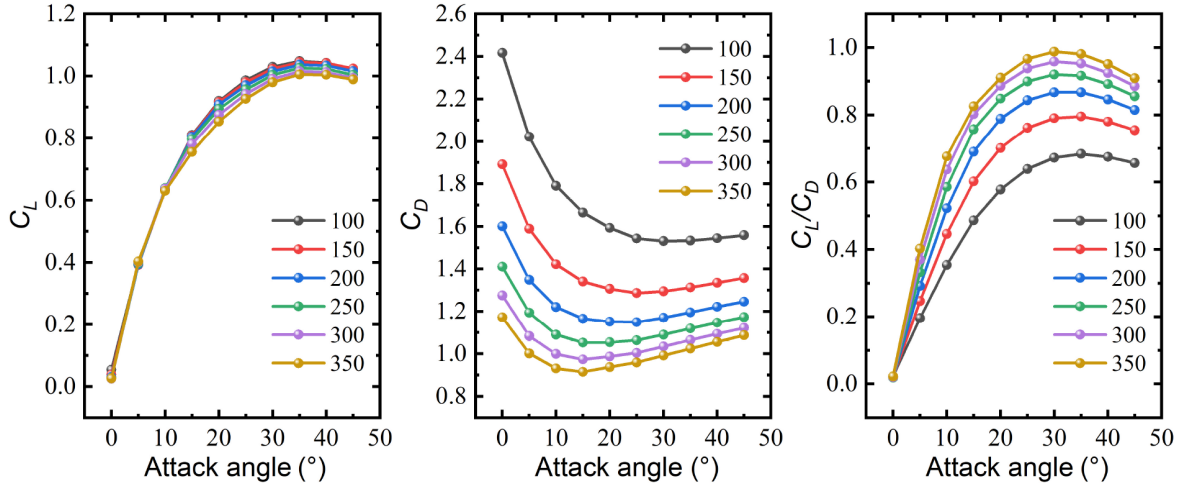

Figure 13 Drag and lift coefficients and lift-to-drag ratio of the virtual barrier model at $\alpha = 30°$ and $\beta = -5°$ for different angles of attack and Reynolds numbers: (a) lift coefficient, (b) drag coefficient, (c) lift-to-drag ratio.

which is significantly higher than the typical stall angle (15°-20°) of standard airfoils. This suggests that the dandelion seed may possess enhanced aerodynamic stability, allowing it to sustain flight more effectively. Figure 13(b) presents the drag coefficient of the model as a function of the attack angle across different Reynolds numbers. It demonstrates a general decrease in drag as the attack angle increases, particularly evident at lower Reynolds numbers, such as in the drag curve for $Re = 50$. Figure 13(c) depicts the lift-to-drag ratio as a function of the attack angle, following a trend similar to that of the lift coefficient: an initial increase followed by a decrease. The Reynolds number has a significant effect on the lift-to-drag ratio, with higher Reynolds numbers resulting in larger ratios. It can be seen that, at an attack angle of about 30°, the model not only achieves a higher lift coefficient but also benefits from a reduced drag coefficient, effectively meeting flight performance requirements.

In summary, the virtual barrier model has shown significant aerodynamic adaptability across various angles of attack and Reynolds number conditions. With increasing angles of attack, the model shows excellent performance in lift coefficient and lift-to-drag ratio, and its stall angle is markedly higher than that of traditional wing designs, suggesting greater stability and resistance to stall during high-angle flight. Moreover, the formation of vortex structures and the characteristics of the flow field have substantially enhanced the model's aerodynamic efficiency, reducing viscous drag. Changes in Reynolds number further confirmed the model's adaptability across different flight conditions, offering solid theoretical foundations and data support for the biomimetic design of micro aerial vehicles.

4. Conclusion

This paper proposes a dandelion virtual barrier model based on the virtual barrier theory to describe the outer edge profile of the dandelion seed filament and evaluates the impact of geometric parameters on its aerodynamic performance using CFD. Some key conclusions can be drawn after a comprehensive analysis as follows:

(I) The dandelion virtual barrier model revealed a novel mechanism of the dandelion seeds for generating flight lift force under horizontal lateral inflow, providing new insights into seed dispersal mechanisms.

(II) The key geometric parameters of the dandelion seed shape have been identified, and simulations reveal that within the parameter range of $\beta = -10°$-$0°$ and $\alpha = 25°$-$30°$, the virtual barrier model achieves optimal aerodynamic performance.

(III) Compared to traditional wing designs, the morphological profile of dandelion seeds has a larger stall angle, thereby increasing the effective angle range for wind-dispersed seeds.

These findings not only provide new perspectives for the design of micro air vehicles but also offer new ideas for understanding biological flight behaviors in nature and designing biomimetic micro air vehicles. However, there are still many avenues for future research. For example, further studies could explore the impact of different flow conditions (such as turbulence or non-uniform wind fields) on the aerodynamic characteristics of dandelion seeds. Additionally, experimental studies and the development of actual prototypes will help validate the effectiveness of the virtual model and advance its potential for engineering applications. Finally, by integrating advanced materials science and manufacturing techniques, more efficient biomimetic micro aerial vehicles can be designed, further advancing this field.

Conflict of interest *On behalf of all authors, the corresponding author states that there is no conflict of interest.*

Author contributions ***Lang Qin:*** *Investigation, Formal analysis, Validation, Writing – original draft.* ***Huasong Qin:*** *Methodology, Resources, part of Visualization, Writing – review & editing.* ***Lifeng Ma:*** *Conceptualization, Project administration, Funding acquisition, Supervision, Writing – review & editing.*

Acknowledgements *This work was supported by the Sir Joseph Pope Fellowship from Nottingham University, the High Performance Computing Platform of Xi'an Jiaotong University, and the National Natural Science Foundation of China (Grant Nos. 12072254, 12102323, and 12472108).*

1 T. Chen, and S. Lan, Numerical analysis of dynamic stability of falling maple samaras, Acta Mech. Sin. **38**, 322111 (2022).
2 B. W. Zhu, and Y. L. Yu, Aerodynamic analysis of bionic cylindrical rib-supporting wings in plunging and flapping motions, Acta Mech. Sin. **39**, 322495 (2023).
3 X. He, Y. Liu, Y. Chen, and S. Wang, Wake of a bio-inspired flapping wing with morphing wingspan, Acta Mech. Sin. **39**, 323061 (2023).
4 Y. Wang, X. He, G. He, Q. Wang, L. Chen, and X. Liu, Aerodynamic performance of the flexibility of corrugated dragonfly wings in flapping flight, Acta Mech. Sin. **38**, 322038 (2022).
5 E. J. Shields, J. T. Dauer, M. J. VanGessel, and G. Neumann, Horseweed (Conyza canadensis) seed collected in the planetary boundary layer, Weed Sci. **54**, 1063 (2006).
6 M. Seale, and N. Nakayama, From passive to informed: Mechanical mechanisms of seed dispersal, New Phytol. **225**, 653 (2020).
7 S. Poppinga, A. S. Böse, R. Seidel, L. Hesse, J. Leupold, S. Caliaro, and T. Speck, A seed flying like a bullet: Ballistic seed dispersal in Chinese witch-hazel (*Hamamelis mollis* OLIV., Hamamelidaceae), J. R. Soc. Interf. **16**, 20190327 (2019).
8 R. Å. Norberg, Autorotation, self-stability, and structure of single-winged fruits and seeds (samaras) with comparative remarks on animal flight, Biol. Rev. **48**, 561 (1973).
9 R. A. Stevenson, D. Evangelista, and C. V. Looy, When conifers took flight: A biomechanical evaluation of an imperfect evolutionary takeoff, Paleobiology **41**, 205 (2015).
10 J. Rabault, R. A. Fauli, and A. Carlson, Curving to fly: Synthetic adaptation unveils optimal flight performance of whirling fruits, Phys. Rev. Lett. **122**, 024501 (2019).
11 C. Cummins, M. Seale, A. Macente, D. Certini, E. Mastropaolo, I. M.

Viola, and N. Nakayama, A separated vortex ring underlies the flight of the dandelion, Nature **562**, 414 (2018).
12 F.-S. Qiu, T.-B. He, and W.-Y. Bao, Effect of porosity on separated vortex rings of dandelion seeds, Phys. Fluids. **32**, 113104 (2020).
13 Y. Shigenaga, and H. Hasegawa, Wake flow visualization of a dandelion pappus with posture change, J. Fluid Sci. Tech. **18**, JFST0019 (2023).
14 Q. Meng, Q. Wang, K. Zhao, P. Wang, P. Liu, H. Liu, and L. Jiang, Hydroactuated configuration alteration of fibrous dandelion pappi: Toward self-controllable transport behavior, Adv. Funct. Mater. **26**, 7378 (2016).
15 M. Seale, O. Zhdanov, M. B. Soons, C. Cummins, E. Kroll, M. R. Blatt, H. Zare-Behtash, A. Busse, E. Mastropaolo, J. M. Bullock, I. M. Viola, and N. Nakayama, Environmental morphing enables informed dispersal of the dandelion diaspore, eLife **11**, e81962 (2022).
16 B. H. Sun, and X. L. Guo, Aerodynamic shape and drag scaling law of a flexible fibre in a flowing medium, Theor. Appl. Mech. Lett. **13**, 100397 (2023).
17 L. Qin, Z. Jian, Y. Xu, and L. Ma, On the attitude stability of flying dandelion seeds, Phys. Fluids. **35**, 081904 (2023).
18 P. G. Ledda, E. Boujo, S. Camarri, F. Gallaire, and G. A. Zampogna, Homogenization-based design of microstructured membranes: Wake flows past permeable shells, J. Fluid Mech. **927**, A31 (2021).
19 Y. Dong, Y. Ni, K. Hu, and T. Zhang, Transition to turbulence in the wake of dandelion-like spoke disk, Phys. Fluids. **35**, 104113 (2023).
20 G. Davidi, and D. Weihs, Flow around a comb wing in low-Reynolds-number flow, AIAA J. **50**, 249 (2012).
21 D. Weihs, and E. Barta, Comb wings for flapping flight at extremely low Reynolds numbers, AIAA J. **46**, 285 (2008).
22 C. P. Ellington, Wing mechanics and take-off preparation of *Thrips* (Thysanoptera), J. Exp. Biol. **85**, 129 (1980).
23 H. Takahashi, A. Isozaki, K. Matsumoto, and I. Shimoyama, in A cantilever with comb structure modeled by a bristled wing of thrips for slight air leak: Proceedings of the 28th IEEE International Conference on Micro Electro Mechanical Systems (MEMS), Estoril, 2015.
24 E. Barta, and D. Weihs, Creeping flow around a finite row of slender bodies in close proximity, J. Fluid Mech. **551**, 1 (2006).
25 E. Barta, Motion of slender bodies in unsteady Stokes flow, J. Fluid Mech. **688**, 66 (2011).
26 S. K. Jones, Y. J. J. Yun, T. L. Hedrick, B. E. Griffith, and L. A. Miller, Bristles reduce the force required to 'fling' wings apart in the smallest insects, J. Exp. Biol. **219**, 3759 (2016).
27 Y. Jiang, P. Zhao, X. Cai, J. Rong, Z. Dong, H. Chen, P. Wu, H. Hu, X. Jin, D. Zhang, and H. Liu, Bristled-wing design of materials, microstructures, and aerodynamics enables flapping flight in tiny wasps, Iscience **25**, 103692 (2022).
28 S. H. Lee, and D. Kim, Aerodynamic response of a bristled wing in gusty flow, J. Fluid Mech. **913**, A4 (2021).
29 S. H. Lee, M. Lee, and D. Kim, Optimal configuration of a two-dimensional bristled wing, J. Fluid Mech. **888**, A23 (2020).
30 M. Lee, E. Mahravan, and D. Kim, Flow-induced rearrangement of a poroelastic cluster, J. Fluid Mech. **983**, A34 (2024).

侧风条件下蒲公英种子形态特征对飞行升力的影响

秦琅, 覃华松, 马利锋

摘要 蒲公英种子凭借其独特的形态特征在空气动力学领域备受关注. 然而, 现有研究主要集中于蒲公英种子在下落过程中的飞行特性, 特别强调其复杂的纤毛结构对尾涡形成的影响, 对于蒲公英种子在侧风条件下由于其形态特征产生的飞行升力的研究仍相对有限. 本研究采用一种新颖的虚拟屏障模型来研究蒲公英种子的空气动力学行为. 该模型基于纤毛外部轮廓的规律性和它们柱状排列产生的虚拟屏障效应而提出. 通过精细的数值模拟, 研究发现蒲公英种子的形态特征在侧风条件下具有优异的空气动力学性能, 尤其是在产生升力方面. 这一特性是蒲公英种子进行远距离传播的关键机制. 此外, 研究进一步考察了模型典型角度下在不同入流攻角下的空气动力学性能, 为理解蒲公英种子在自然环境中的飞行特性提供了新视角. 这些发现不仅对外部空气动力学领域的研究具有一定价值, 也为工程领域中潜在的生物仿生应用提供了有益的启示.